PNAS
www.pnas.org

Supplementary Information for

Fundamental Helical Geometry Consolidates the Plant Photosynthetic Membrane

Yuval Bussi, Eyal Shimoni, Allon Weiner, Ruti Kapon, Dana Charuvi, Reinat Nevo, Efi Efrati, and Ziv Reich

Efi Efrati
Email: efi.efrati@weizmann.ac.il

Ziv Reich
Email: ziv.reich@weizmann.ac.il

This PDF file includes:

Other supplementary materials for this manuscript include the following:

www.pnas.org/cgi/doi/10.1073/pnas.1905994116

SI Materials and Methods

Plants

Mature *Lactuca sativa L.* (lettuce) plants were obtained from an organic field. The plants were transferred to a growth room where they were kept under short-day conditions (10/14-h light/ dark cycles) at 22°C and 80 µmol photons$\times m^{-2} \times s^{-1}$ for 2-3 days. Prior to the experiments, plants were dark-adapted overnight.

Electron Tomography

Dual-axis STEM tomography. Sections, ranging from *ca.* 500 to *ca.* 700 nm in thickness, were cut with a Leica Ultracut UCT microtome, using a Diatome diamond knife, and subsequently decorated with 10-nm colloidal gold markers and double-stained with 2% uranyl acetate in 50% ethanol followed by Reynold's lead citrate. Dual-axis tilt series were acquired on FEI Tecnai F20 operating in nanoprobe STEM mode at 200 kV and condenser aperture of 10 µm. Images were recorded with a Gatan axial bright-field STEM detector over a tilt range of -65˚ to 64˚ (except for one series that was recorded between -63˚ to 58˚), at 1.5˚ intervals, using the SerialEM software (1).

FIB-SEM tomography. Resin blocks were processed according to (2) with some modifications. Serial views of freshly exposed surfaces were acquired on FEI Helios Nanolab DualBeam, using the Auto Slice-and-View G2 (FEI) software. Combined secondary and backscattered electron images were recorded with 0.34 nA at 2 kV in the immersion lens mode, with pixel size of 1.56 nm. Slices were milled off with an ion beam current of 0.44 nA at 30 kV; the step size was 10 nm.

Image Processing and Analysis

TEM/STEM data. Image alignment and 3D reconstruction were performed using the IMOD image-processing package (3). The TEM serial sections were subsequently aligned into one stack, ca. 1-µm-thick, by manually tracking membrane features consistent to slides preceding and succeeding the section transitions, and then manually aligning the sections using the manual alignment function in the eTomo interface of IMOD.

FIB-SEM data. Images were aligned in ImageJ (79; http://rsb.info.nih.gov/ij/) using the StackReg plugin (80; http://bigwww.epfl.ch/thevenaz/stackreg/). Image enhancement was performed using the automatic Contrast Limited Adaptive Histogram Equalization (CLAHE) plugin (http://rsbweb.nih.gov/ij/plugins/clahe/index) in the FIJI image processing package (6).

For both the tomography and FIB-SEM datasets, image segmentation and subsequent processing were carried out using the Avizo 3D software package (http://www.fei.com/software/avizo3d). Image segmentation was performed using multiple materials and the magic wand, blow, and brush tools. The segmented results were rendered into 3D surfaces and inspected using the oblique slice feature. Surface statistics were exported from Avizo and analyzed using the MATLAB and Statistics Toolbox Release 2018a (7). The ratio of helical junctions per granum was measured in three sections from different chloroplasts. Measurements were carried out using the FIJI image processing package (6). The values for the maximal slit-length and stroma lamellae tilt (away from the grana edges) were obtained from five chloroplasts. For all other statistical means reported in the manuscript, the values were obtained from six chloroplasts. All values shown are means ± SD.

Modeling

Surface energy minimization was performed with Surface Evolver, version 2.70 (8; www.susqu.edu/facstaff/b/brakke/evolver/html/default.htm). The geometric elements of the surface (vertices, edges, facets) are initially defined, as well as surface energies, boundaries, and constraints. All polygons of the surface are triangulated and can be progressively refined to the desired resolution. The program iteratively evolves the surface toward minimal surface energy by a gradient descent method. Since membrane bilayers bend as a unit, we modeled them by sheet planes, similar to the approach taken by Terasaki *et al.* (9). The surfaces were composed of right- and left-handed helical membrane elements, joined together seamlessly at their outer boundaries/interfaces, forming layered sheets. Each helical element was defined by a parameterized internal boundary having a set diameter and pitch. We note that, as our data suggest invariance of geometrical features to the number of layers in the grana stack, we modeled them as columns having effectively infinite height. The resulting minimized surface was exported to Autodesk Maya for 3D rendering.

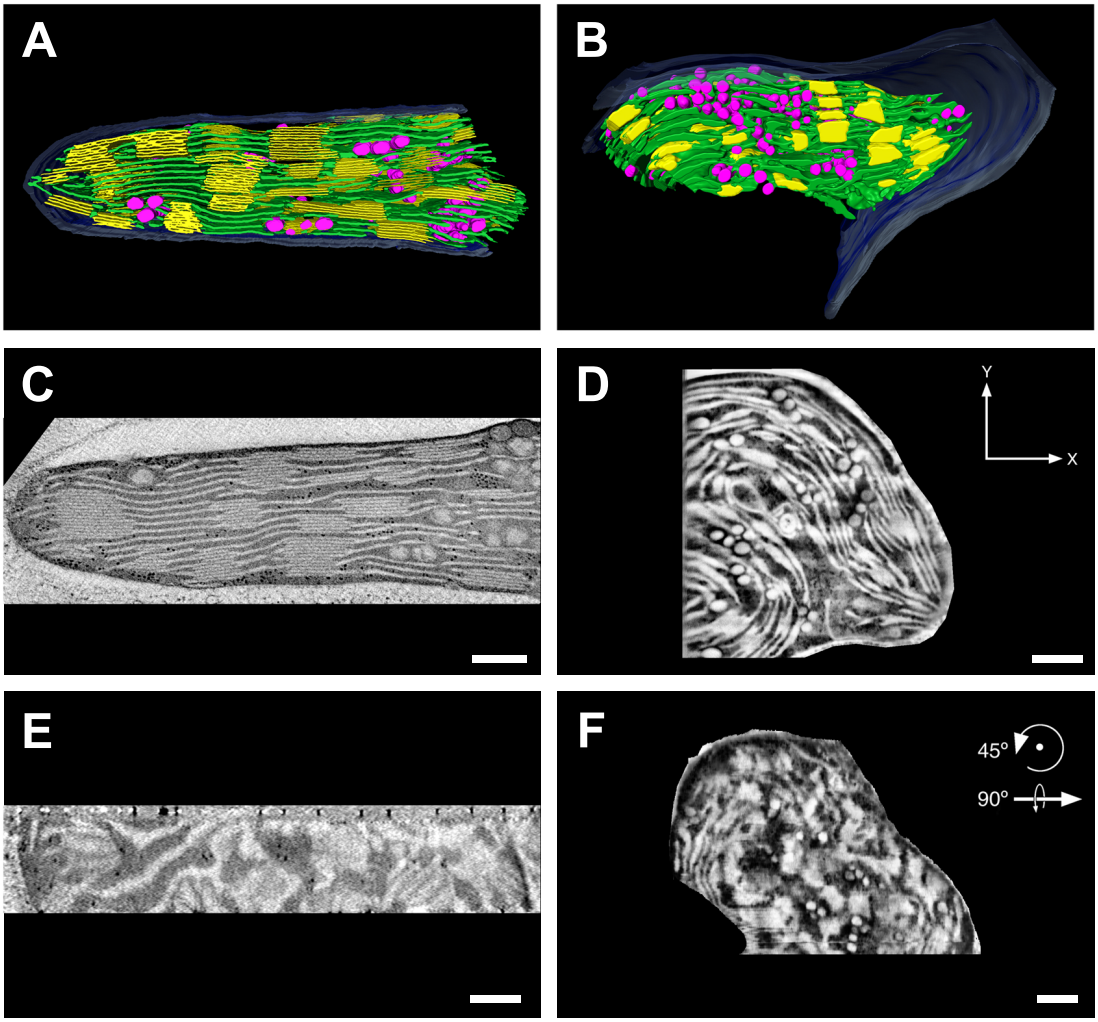

Fig. S1. 3D structure of the thylakoid membrane network in a lettuce chloroplast.

(A, B) Large-scale 3D models generated from segmentation of tomographic reconstructions by STEM **(A)** and FIB-SEM **(B)**. Grana and stroma thylakoids are shown in yellow and green, respectively; the chloroplast envelope is shown in blue and the magenta-colored bodies are plastoglobules. **(C-F)** 10-nm-thick tomographic slices presented roughly perpendicular **(C, D)** or parallel **(E, F)** to the plane of the grana layers. **(C, E)** Bars = 250 nm. **(D, F)** Bars = 500 nm.

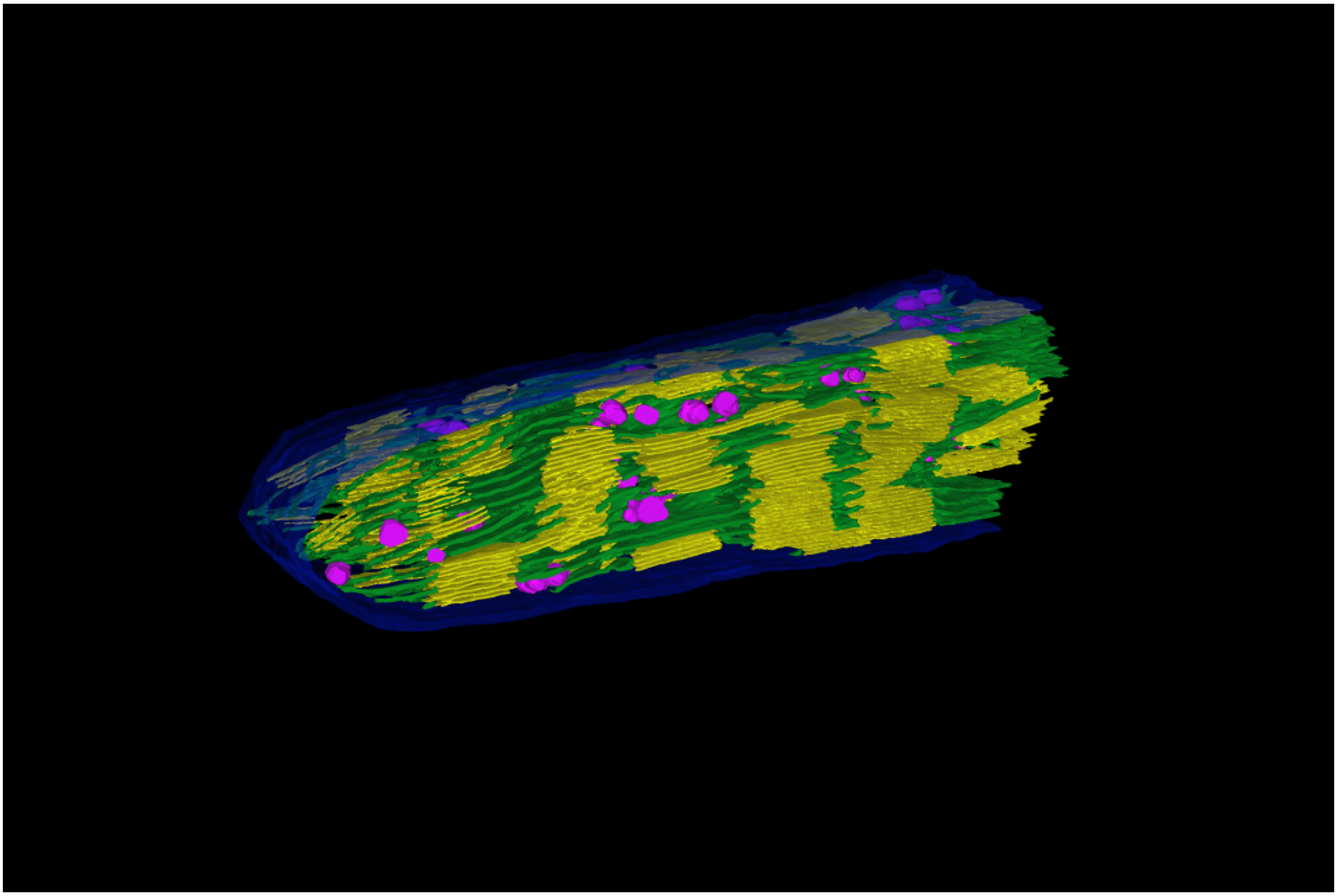

Fig. S2. The overall 3D structure of a plant thylakoid membrane network.

A three-dimensional model generated by segmentation of tomographic reconstruction by STEM, presented in SI Appendix, Fig S1A. [For interactive 3D visualization open with compatible software, such as Adobe® Acrobat Reader®, freely available at get.adobe.com/reader/.]

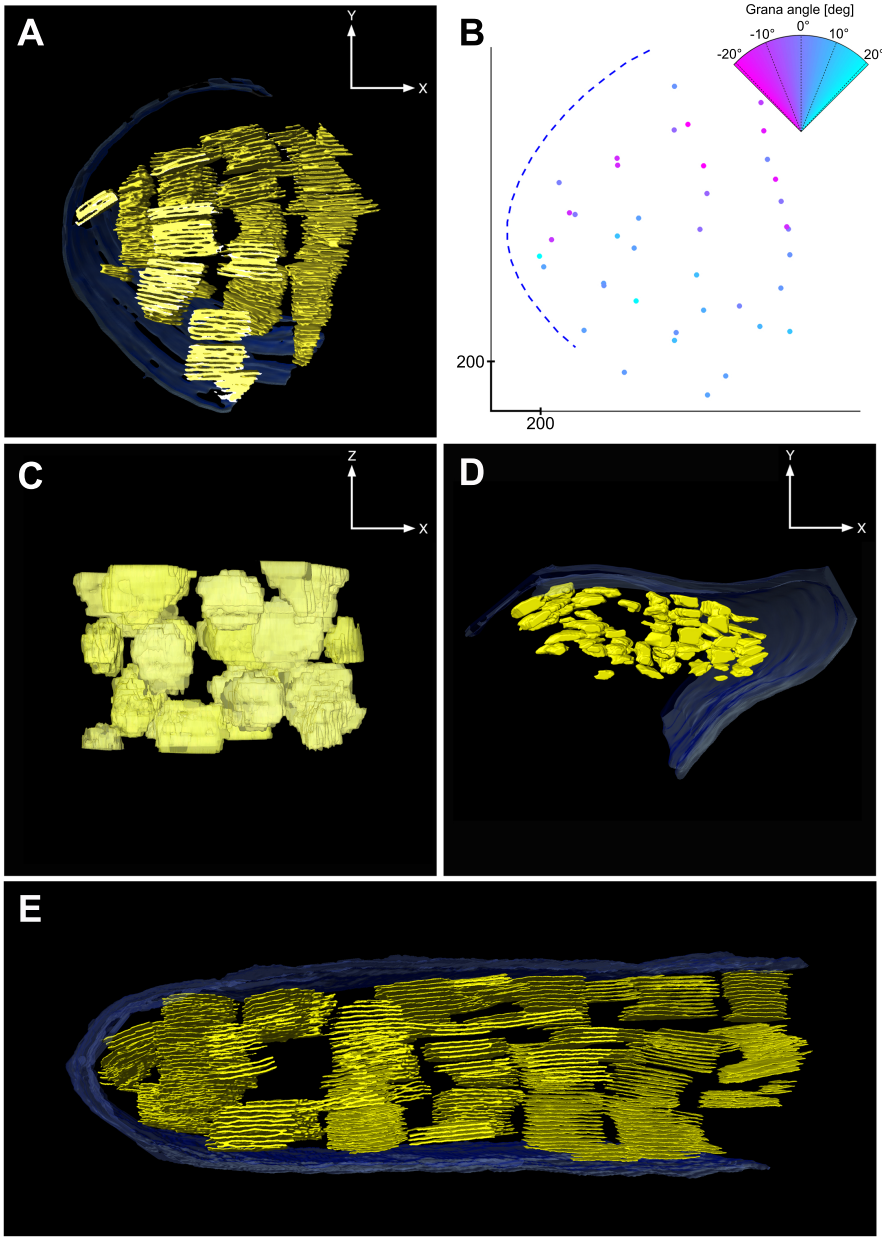

Fig. S3. Grana are stacked into compound columns.

(A, C, D, E) 3D models generated from tomographic reconstructions by TEM **(A, C)**, FIB-SEM **(D)**, and STEM **(E)**, with only grana thylakoids (yellow) and the chloroplast envelope (blue) depicted. **(C)** Top view of the grana shown in **(A)** rotated 90º about the *x*-axis with the chloroplast envelope removed. **(B)** A plot of the center locations of the grana from **(A)** with axes corresponding to position in the *x*-*y* plane (Bars = 200 nm). The center location is defined as the midpoint of the middle granum layer in the stack. The color of the data points indicates the angle of the grana with respect to the *y*-axis, as shown in the wedge at the top right. The blue dotted line demarcates the boundary of the chloroplast envelope.

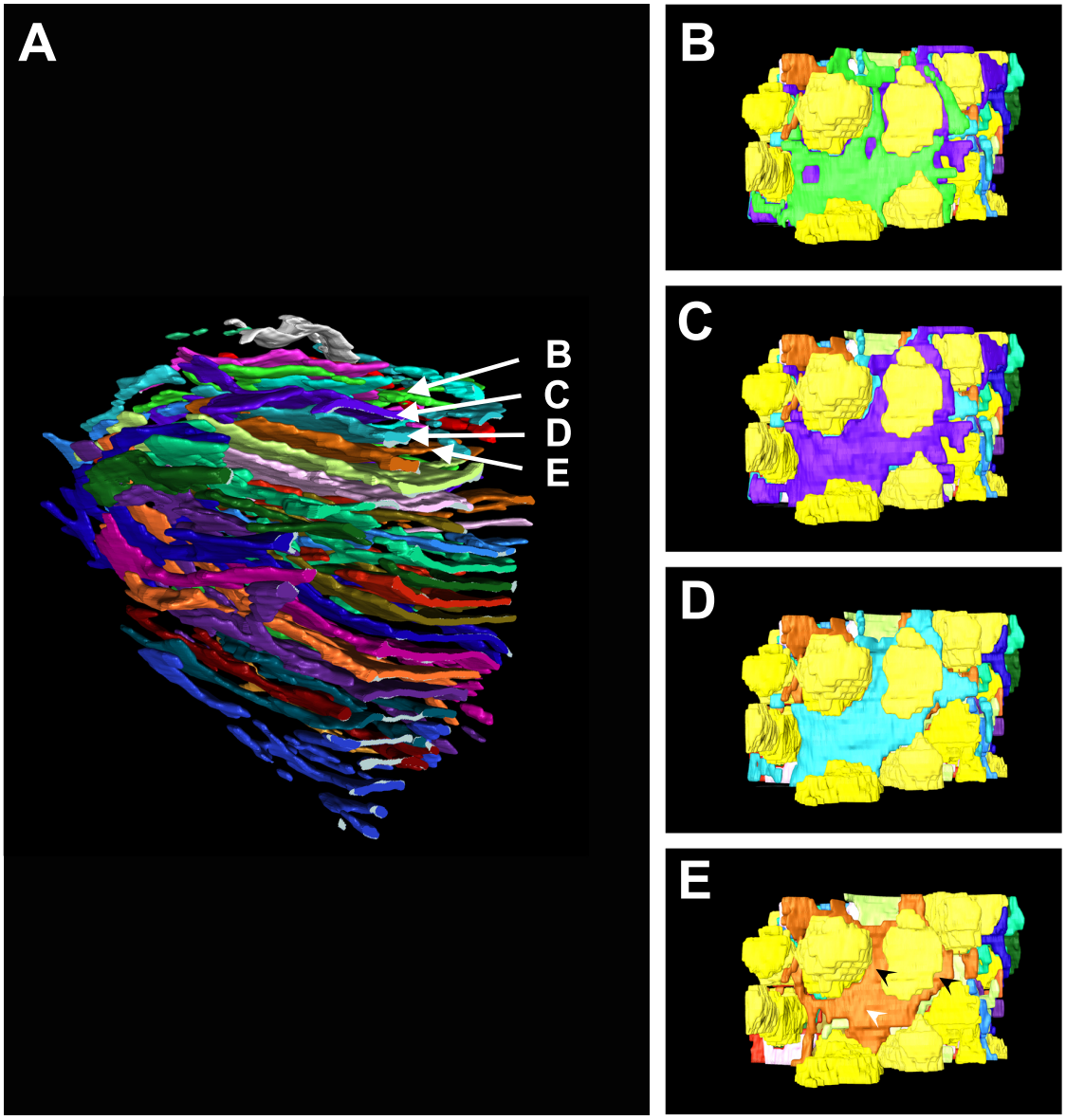

Fig. S4. Parallel-sheet organization of the stroma lamellae.

(A) 3D tomographic model with only stroma lamellae visible (a part of this model is also shown in Fig. 2F). Individual sheets are colored differently. **(B-E)** Top views of the model above the positions indicated by the corresponding arrows in **(A)**; *e.g.,* in panel **(E)** all stroma lamellar sheets above the orange one pointed to have been removed. Grana stacks are shown in yellow. **(E)** When the grana are very close to each other, the sheet-like structure (white arrowheads) of the stroma thylakoids takes on a tubular morphology (black arrowheads; see also 10). Note that the thylakoid network is fully interconnected, and the separate segmentation of different layers serves to demonstrate the long-range parallel sheets characteristic of the stroma lamellae, as seen from this top view.

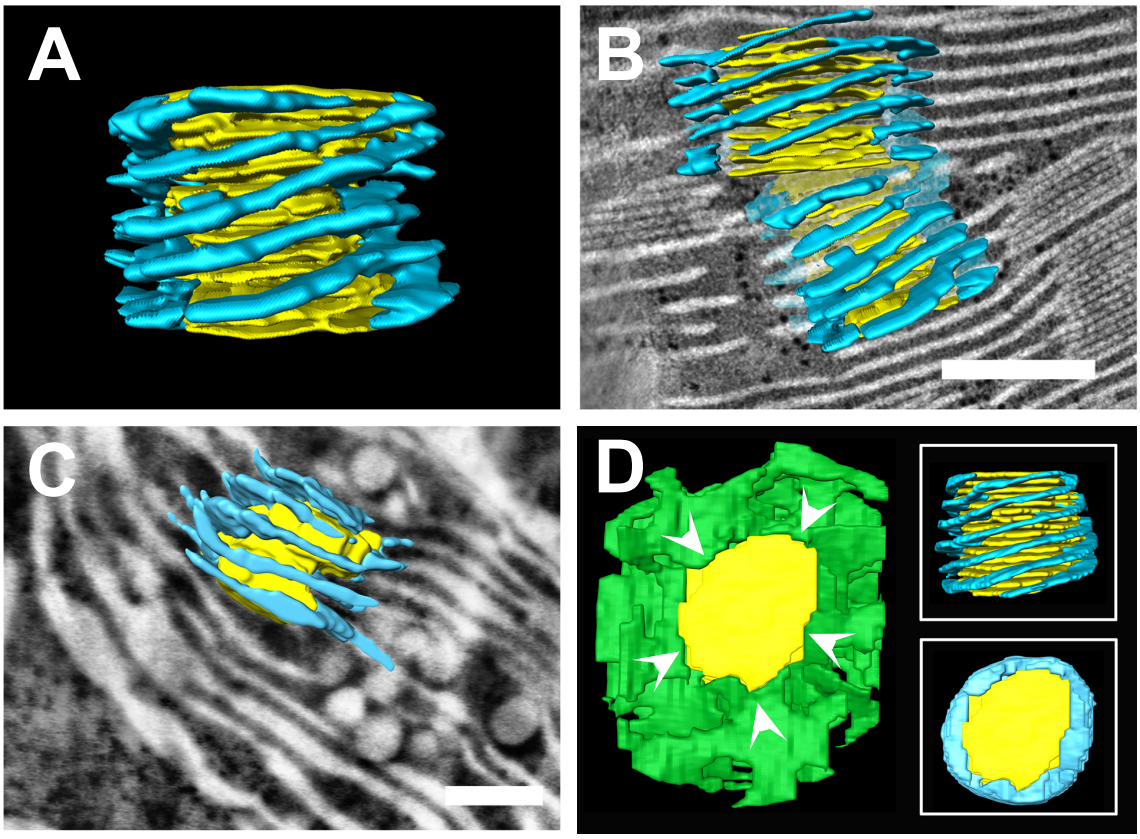

Fig. S5. Right-handed helices surrounding the grana.

(A-D) 3D models generated by segmentation of tomographic reconstructions by TEM **(A, B)**, FIB-SEM **(C)**, and STEM **(D)** showing right-handed helices (light blue) that surround the grana (yellow). **(D)** From the top view, radial connections of five helices to the top grana disc are marked (white arrowheads). For this model, a wider radius around the granum was also segmented with all the stroma lamellae colored green. **(D inset)** The helices surrounding the grana are shown from the top and side views. In **B** and **C**, the models are superimposed on ~10-nm-thick tomographic slices. To the right of the top granum in **(B)**, parallel lines of stroma lamellae represent sheets that extend outward and which are directly connected to the helices that surround the granum (see Figs. 4, 7, and 8). To the left of the bottom granum therein, the stroma lamellae are discontinuous in 2D due to the presence of a stroma lamellar junctional site (see Figs. 4 and 8). Bars = 250 nm.

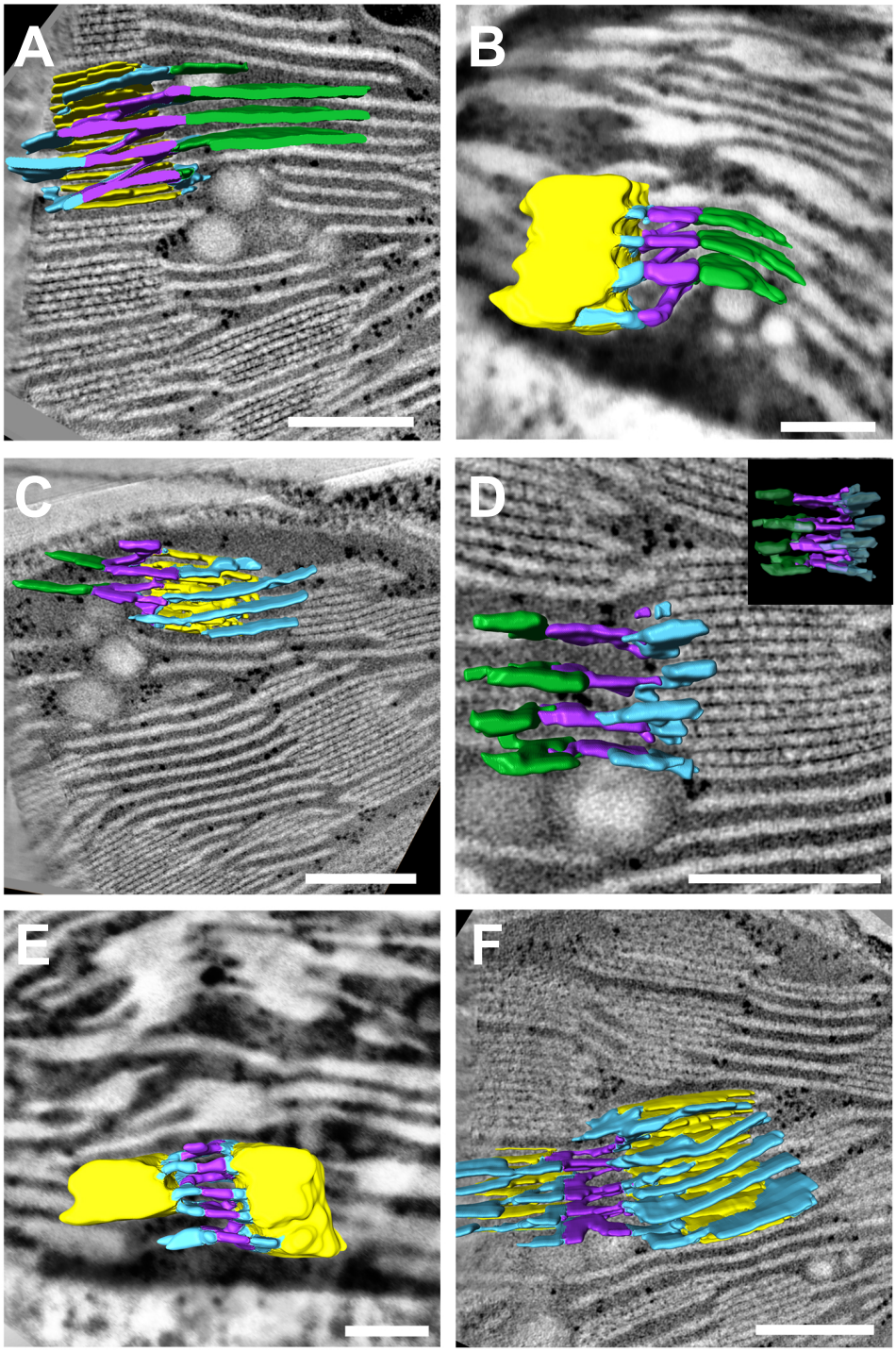

Fig. S6. Left-handed helical junctions.
(A-F) 3D models generated from tomographic reconstructions by TEM **(A, C, D, F)** and FIB-SEM **(B, E)**, showing left-handed helical surfaces (purple), connecting right-handed helices (light blue) that surround the grana (yellow) to the stroma lamellar sheets (green) **(A-D),** or to right-handed helices of adjacent grana **(E, F)**. Bars = 250 nm.

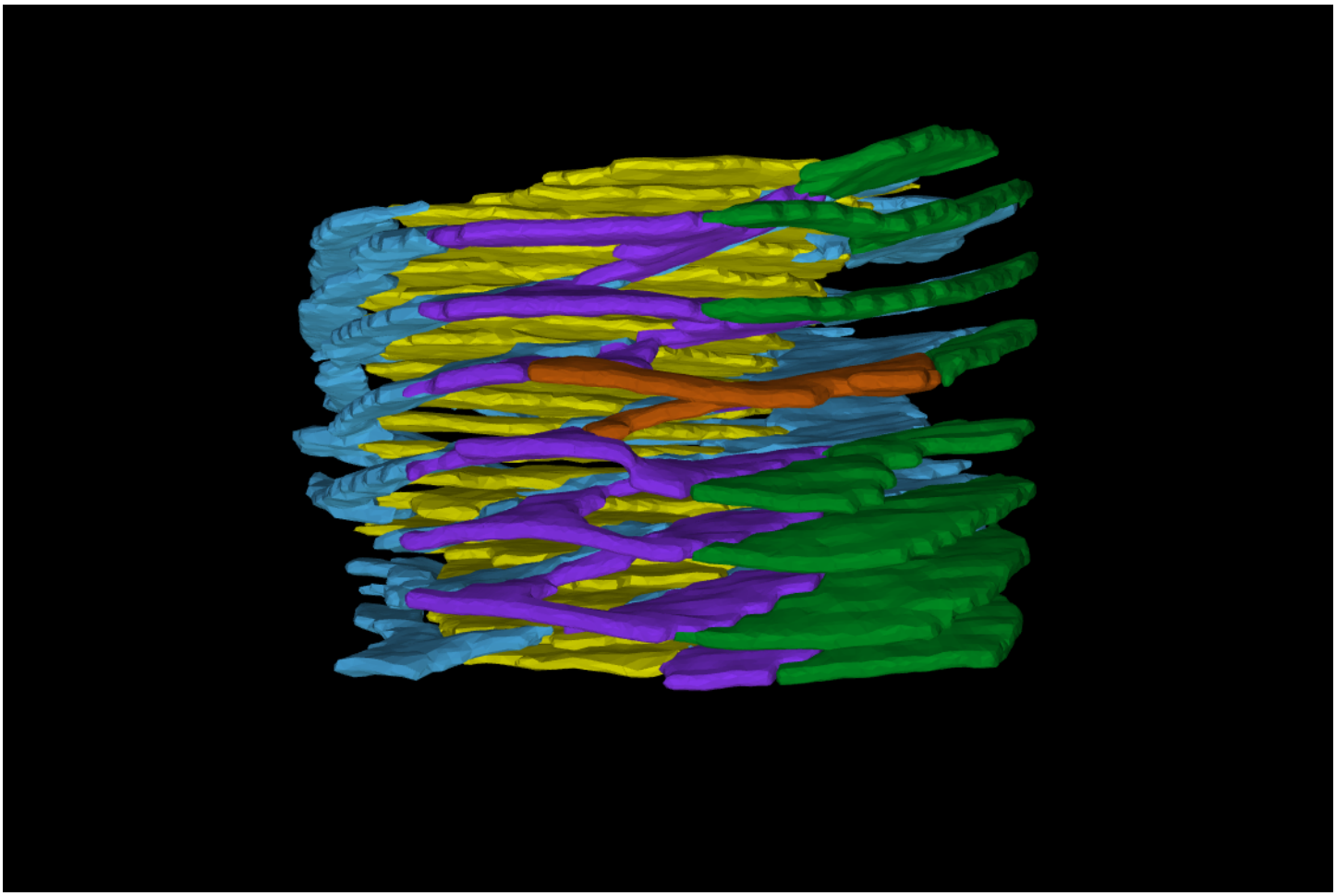

Fig. S7. The 3D structure of a grana-stroma assembly with one helical junction.

A three-dimensional model generated by segmentation of tomographic reconstruction by STEM, presented in Fig 4I. Left-handed helical surfaces (purple) connect between the stroma lamellar sheets (green) and the right-handed helices (light blue) that surround the grana (yellow). One of the bifurcations is segmented in orange. [For interactive 3D visualization open with compatible software, such as Adobe® Acrobat Reader®, freely available at get.adobe.com/reader/.]

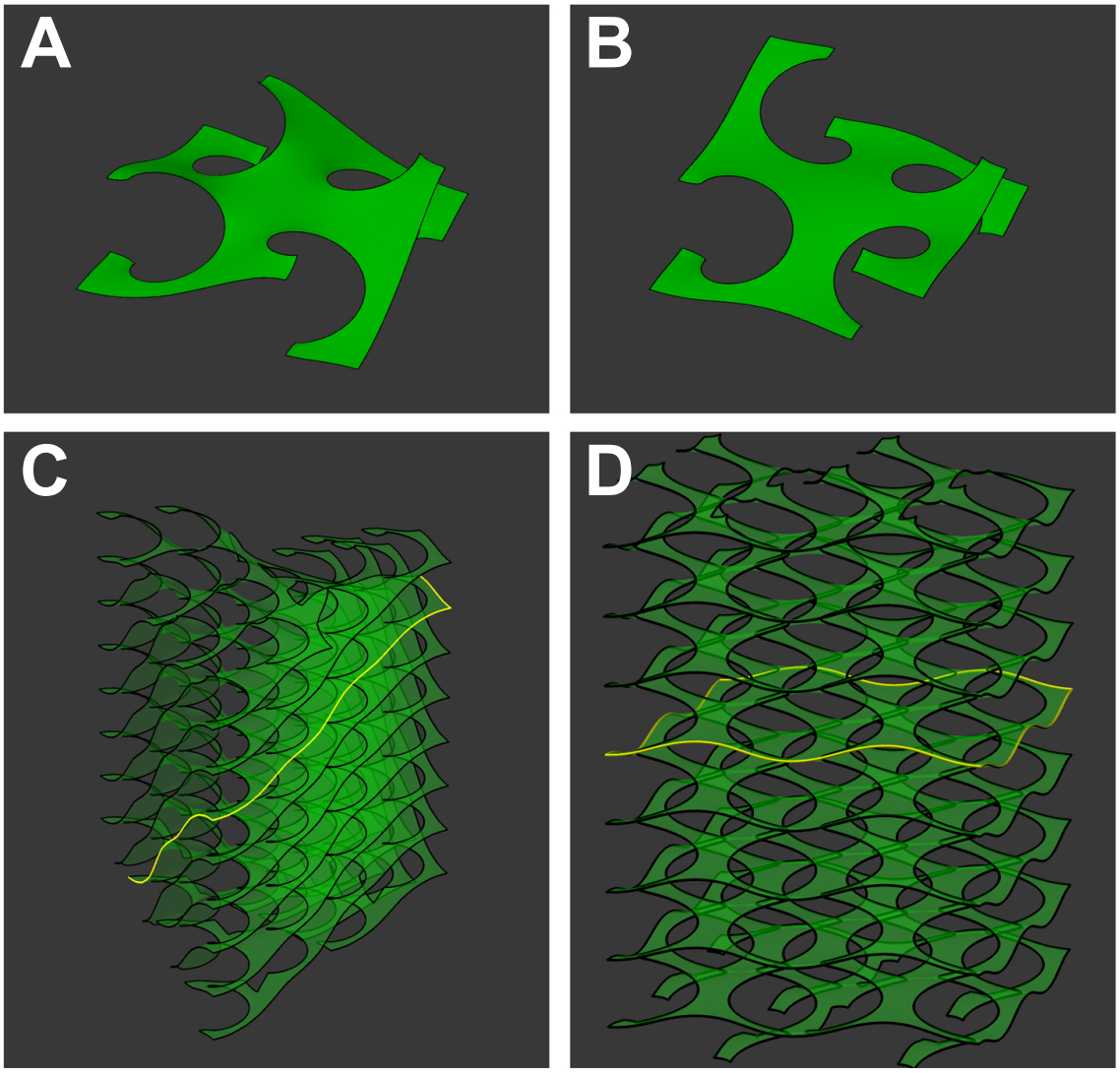

Fig. S8. Sheet orientations resulting from alternative helical connections.

(A, B) Arrays of interconnected basic helical membrane elements of varying handedness: **(A)** All right-handed. **(B)** Alternating left- and right-handed. **(C, D)** Arrayed networks comprised of 4x4 columns and 8 sheets corresponding to the different basic units shown in **(A, B)** and Fig. 5 B and D, respectively, each eight sheets high. In each panel, the edge of one lamellar sheet is highlighted in yellow. For clarity, grana cylinders are not shown. **(C)** When all helical elements have the same handedness, the lamellar sheets are sloped at the edges (forming a helix around the network). **(D)** Alternating handedness along both the *x*- and *y*-axes allows the stroma lamellae to remain parallel and aligned to the grana layers. This arrangement, which is the one observed in the reconstructed structures, corresponds to a minimum of surface and elastic bending energy of the membrane network.

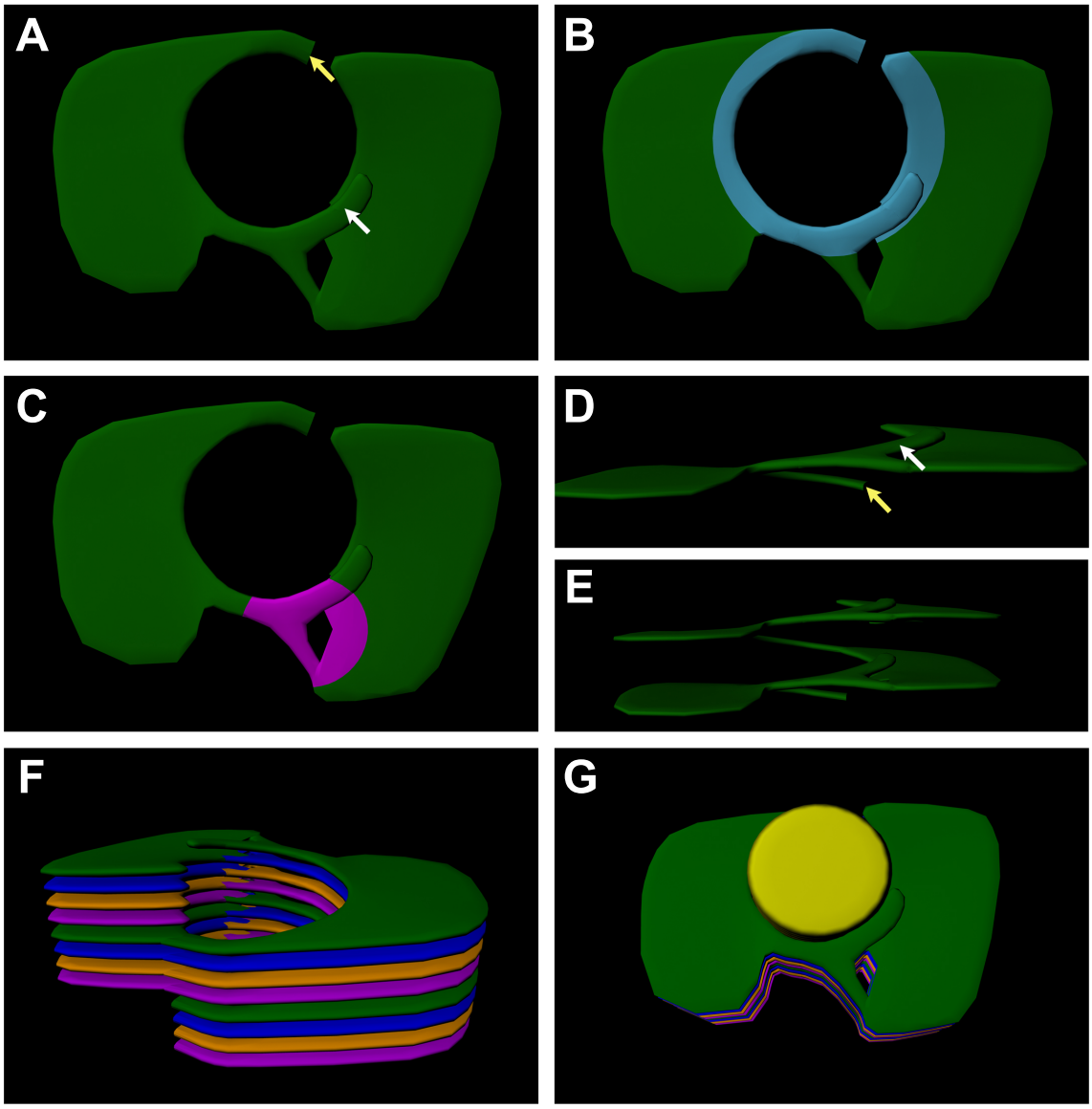

Fig. S9. Repeating elements of the granum-stroma assembly.

The stroma lamellae of the idealized model (Fig. 7) is partitioned into repeating elements. One such unit is shown in panel **(A)**. The unit is essentially a perforated sheet with an overgrowth (white arrow), which connects it to the unit above. At the perforation, the edges connect to units located four levels above or below (yellow arrows). A side view of these latter connections is provided in **(D, E)**. **(B)** The inner edges of the perforation (light blue) make up the right-handed helices that surround the grana. Note that the overgrowth continues along a parallel helix one level above the inner edge of the right half of the unit. This can be seen more clearly in the side view shown in **(E)**. **(C)** The left-handed helical junctions (purple) are essentially formed by the connections between the overgrowths on different levels. In panel **F**, the model is expanded to include eight units comprising of four intertwined right-handed helices connected to the flanking sheets, directly, by

virtue of transformation, and indirectly, through a left-handed helical junction. **(G)** Top-view of the assembly shown in F with a granum stack added (yellow). Note the channel formed by the left-handed helical junction.

Movie S1. The 3D architecture of the plant thylakoid membrane.
Shown are tomographic slices through the model presented in Fig. 2A.

SI References

1. Mastronarde DN (2005) Automated electron microscope tomography using robust prediction of specimen movements. *J Struct Biol* 152(1):36–51.
2. Bennett AE, et al. (2009) Ion-abrasion scanning electron microscopy reveals surface-connected tubular conduits in HIV-infected macrophages. *PLoS Pathog* 5(9):e1000591.
3. Kremer JR, Mastronarde DN, McIntosh JR (1996) Computer visualization of three-dimensional image data using IMOD. *J Struct Biol* 116(1):71–76.
4. Rasband WS (1997) ImageJ. Available at: https://imagej.nih.gov/ij/.
5. Thévenaz P, Ruttimann UE, Unser M (1998) A Pyramid Approach to Subpixel Registration Based on Intensity. *IEEE Trans Image Process* 7(1):27–41.
6. Schindelin J, et al. (2012) Fiji: an open-source platform for biological-image analysis. *Nat Methods* 9(7):676–682.
7. MATLAB and Statistics Toolbox.
8. Brakke KA (1992) The Surface Evolver. *Exp Math* 1(2):141–165.
9. Terasaki M, et al. (2013) Stacked endoplasmic reticulum sheets are connected by helicoidal membrane motifs. *Cell* 154(2):285–96.
10. Austin JR, Staehelin LA (2011) Three-Dimensional Architecture of Grana and Stroma Thylakoids of Higher Plants as Determined by Electron Tomography. *PLANT Physiol* 155(4):1601–1611.